



Cite this: DOI: 10.1039/c8nj04585b

Highly active enzymes immobilized in large pore colloidal mesoporous silica nanoparticles†

 Dorothée Gößl,^{id} Helena Singer, Hsin-Yi Chiu, Alexandra Schmidt,
Martina Lichtnecker, Hanna Engelke^{id} and Thomas Bein^{id}*

Various bio-applications of mesoporous materials (e.g., the immobilization of enzymes or the delivery of biomolecules such as siRNA) require large pores for the successful adsorption of the rather large molecules of interest and protecting the fragile cargo from external forces such as degradation. We describe the facile synthesis of functionalized mesoporous silica nanoparticles with large pores (LP-MSNs) providing high loading capacity for the immobilization of two differently-sized enzymes. The synthesis procedure yields homogeneous core-shell particles of about 100 nm in size with large mesopores (about 7 nm in diameter) and an azide-functionality inside the pores. The LP-MSNs were synthesized employing a co-condensation approach with the rather large micellar template cetyltrimethylammonium *p*-toluenesulfonate (CTATos). Due to the azide functionality, the LP-MSNs are suitable for bio-orthogonal click chemistry reactions within the porous network. Two different acetylene-functionalized enzymes (sp-carbonic anhydrase (CA) and sp-horseradish peroxidase (HRP)) were immobilized in the pores of the obtained LP-MSNs by a copper-catalyzed 1,3-dipolar cycloaddition reaction. The covalent attachment of the enzymes within the mesopores allowed us to investigate the catalytic performance of the enzyme-silica systems. The enzymes are stable after bioconjugation with the silica support and show high catalytic activity over several cycles for the colorimetric reaction of guaiacol (2-methoxyphenol) in case of LP-MSN-HRP and the hydrolysis of 4-nitrophenyl acetate (NPA) by LP-MSN-CA.

Received 9th September 2018,
Accepted 3rd December 2018

DOI: 10.1039/c8nj04585b

rsc.li/njc

Introduction

Ordered mesoporous silica materials have attracted increasing attention due to the ability to tailor the structural and textural features including particle size, pore size, pore volume and surface area.^{1–6} With the possibility to introduce various functionalities into the mesoporous framework, these materials have turned into interesting candidates for various biotechnological applications.^{4,7–10} However, such applications often involve fairly large molecules of more than 5 nm in size that may not fit into the pores of established silica nanoparticles (*ca.* 4 nm). Additionally, the active molecules need to be immobilized while preserving their function.

Considerable efforts have been made in the past years regarding the control of mesostructural diversity, compositional flexibility and morphology during the synthesis of mesoporous silica nanoparticles (MSNs).^{3,11–13} In recent years the synthesis of well-defined large-pore mesoporous systems with small particle sizes (in the size-range of 100–200 nm) for the

encapsulation of large biomolecules (*i.e.* enzymes or siRNA) has been addressed.^{14–17} Recently, the group of Zhang published a synthesis route for wide-pore stellate MSNs *via* the use of cetyltrimethylammonium *p*-toluenesulfonate (CTATos) as template in a near-neutral precursor solution.¹⁸ The resulting stellate particles show a pore size distribution between 10 to 20 nm and a defined particle size of around 100 nm. With those properties they represent an ideal delivery vehicle for the cellular transport of large-sized biomolecules.¹⁹

Here, we describe a delayed co-condensation approach to create spatially segregated core-shell phenyl- and azide-functionalized large-pore MSNs (LP-MSNs), which serve as a versatile platform for the immobilization of enzymes. Due to their large pores, our functionalized LP-MSNs can be loaded with large bioactive molecules and thus are promising candidates for numerous bio-applications, including biocatalysis.

A promising way to introduce enzymes as biocatalysts in industrial applications is their immobilization onto inorganic mesoporous supports.^{2,20–22} Organo-functionalized nanostructured mesoporous silica materials have attracted great attention among the available inorganic host systems as they offer outstanding properties for the immobilization and encapsulation of biomolecules.^{2,23,24} As the pores of LP-MSNs match the size of enzymes, such silica materials are excellent candidates

Department of Chemistry and Center for NanoScience (CeNS), University of Munich (LMU), Butenandtstrasse 5–13(E), 81377 Munich, Germany. E-mail: bein@lmu.de

† Electronic supplementary information (ESI) available: Fig. S1–S11 (additional characterization) and calculation A1. See DOI: 10.1039/c8nj04585b

for enzyme immobilization,²⁵ yet their potential in this field still needs to be explored. Previous studies on established mesoporous silica materials (*e.g.* SBA-15) revealed that enzyme confinement within such hosts can increase the stability and reduce denaturation by protein unfolding, one major issue in industrial applications of biocatalysts.²⁶ However, as a consequence of immobilization onto the solid support, a decrease of the enzymatic activity relative to the free enzyme is often observed in such systems.^{27,28} Strong interactions between enzymes and the host materials can be controlled by complementary organo-functionalization of the porous network, resulting in different catalytic activity and loading capacities.^{29–31} As the functionalization of the mesoporous framework can be easily modified, the organo-moieties can be adjusted to the requirements of the respective enzyme and the preferred attachment reaction.

Furthermore, the application of mesoporous silica supports allows for the adjustment of pore- and particle size, structural arrangement and surface properties to optimize loading capacity and enzyme activity.^{8,32,33} Lee *et al.* have reviewed different methods of covalent enzyme immobilization onto mesoporous silica supports.³⁴ Here, we use the flexibility of silica functionalization for loading active enzymes and our newly developed MSNs with large pores to immobilize enzymes while retaining their activity. Additionally, we make use of the demonstrated reusability of immobilized horseradish peroxidase in SBA-16 to be able to study the catalytic behaviour and improved stability over more than one cycle.³⁵ Previous studies describe the immobilization of horseradish peroxidase (HRP) onto the surface of mesoporous silica nanoparticles *via* physical adsorption or covalent binding by using the crosslinker glutaraldehyde.^{36,37} Due to the fact that glutaraldehyde is toxic and rather unstable in air,³⁸ here we use a modified azide-alkyne click chemistry approach established by Schlossbauer *et al.* to immobilize enzymes into the LP-MSNs.^{39,40} This method is biocompatible and avoids unfavorable pore blocking. The same immobilization technique is also used to covalently bind an essential metalloenzyme, namely carbonic anhydrase, to the pore walls of the mesoporous silica nanoparticles. The immobilization of enzymes in general enables their already mentioned reusability and furthermore their long-term use in bioreactors.⁴¹

Two different enzymes, namely the lyase carbonic anhydrase (CA) and the peroxidase horseradish peroxidase (HRP), were chosen for this study and were immobilized with an efficient method into the newly developed azide-functionalized LP-MSNs. A novel co-condensation synthesis approach was developed to generate organo-functionalized MSNs with large pores suitable for biocompatible coupling methods. To study the catalytic activity of the immobilized enzymes, two suitable activity assays were performed. In the case of carbonic anhydrase, the catalyzed hydrolysis of the substrate 4-nitrophenol acetate was studied by following the increasing absorbance of yellow 4-nitrophenol at 400 nm over time. For immobilized horseradish peroxidase, the catalyzed oxidation of guaiacol (2-methoxyphenol) was recorded at a wavelength of 470 nm over time. It was shown that the immobilized enzymes exhibited high stability

and remained highly active after covalent immobilization in the LP-MSNs.

In this work we combine a simple support synthesis with a very efficient immobilization technique to obtain an active, stable and reusable enzyme-silica system.

Materials and methods

Materials

Tetraethyl orthosilicate (TEOS, Aldrich, $\geq 99\%$), phenyltriethoxysilane (PhTES, Aldrich, $> 98\%$), cetyltrimethylammonium *p*-toluenesulfonate (CTATos, Sigma), triethanolamine (TEA, Aldrich, 98%), (3-chloropropyl)triethoxysilane (CPTES, Fluka, 95%), diethyl ether (Et₂O, Sigma, $> 98\%$), sodium azide (Fluka, 99%), ethanol (EtOH, Aldrich, absolute), conc. hydrochloric acid (HCl, Aldrich, 37%), ammonium nitrate (NH₄NO₃, Sigma, 99%), *N*-(3-dimethylaminopropyl)-*N*-ethylcarbodiimide (EDC, Alfa Aesar, 98%), 4-pentynoic acid (Fluka, 97%), tris(hydroxymethyl)aminomethane (TRIS, Sigma, 99.8%), 2-(*N*-morpholino)ethanesulfonic acid (MES, Sigma, 99.5%), carbonic anhydrase from bovine erythrocytes (Sigma, $\geq 95\%$ (SDS-PAGE), specific activity ≥ 3500 W A units per mg protein, lyophilized powder), peroxidase from horseradish (Sigma, Type VI-A, essentially salt-free, lyophilized powder, 950–2000 units per mg solid (using ABTS), ≥ 250 units per mg solid (using pyrogallol)), (+)-sodium L-ascorbate (Sigma, $\geq 98\%$), copper(II) sulfate (Sigma, $\geq 99.99\%$), disodium hydrogen phosphate (Na₂HPO₄, Sigma, $> 99\%$), monosodium hydrogen phosphate (NaH₂PO₄, Sigma, $> 99\%$), sodium hydroxide (1 M, Sigma), dipotassium hydrogen phosphate (K₂HPO₄, Sigma, $> 99\%$), monopotassium hydrogen phosphate (KH₂PO₄, Sigma, $> 99\%$), 4-nitrophenyl acetate (Sigma, esterase substrate), guaiacol (Sigma, oxidation indicator, $\geq 98.0\%$), hydrogen peroxide (Sigma, 30 wt%). Unless otherwise noted, all reagents were used without further purification. Bi-distilled water from a Millipore system (Milli-Q Academic A10) was used for all syntheses and purification steps.

Methods

For transmission electron microscopy, samples were investigated with an FEI Titan 80-300 transmission electron microscope (TEM) operating at 300 kV with a high-angle annular dark field detector. A droplet of the diluted MSN solution in absolute ethanol was dried on a carbon-coated copper grid. The TEM, SEM and STEM micrographs in Fig. 1a–c show template-extracted mesoporous large pore silica particles (LP-MSN-N₃) generated with the above described synthesis procedure (details below). Nitrogen sorption measurements were performed on a Quantachrome Instruments NOVA 4000e and on an Autosorb iQ instrument. All samples with attached enzyme (15 mg each) were treated at 298 K (12 h *in vacuo*), whereas the sample LP-MSN-N₃ was heated to 393 K for 12 h *in vacuo* (10 mTorr) to outgas the samples before nitrogen sorption was measured at 77 K. For calculations of pore sizes and volumes a non-local density functional theory (NLDFT) equilibrium model of nitrogen on silica was used. The obtained physisorption data for

LP-MSN-N₃ are shown in Fig. 1e (nitrogen sorption isotherm) and Fig. 1f (pore size distribution) and in Fig. 2a (isotherms) and Fig. 2b (pore size distribution) for LP-MSN-CA and LP-MSN-HRP. Dynamic light scattering (DLS) measurements were performed on a Malvern Zetasizer-Nano instrument equipped with a 4 mW He-Ne laser (633 nm) and an avalanche photodiode. The hydrodynamic radius of the particles was determined by dynamic light scattering in water. The data are shown in Fig. 1d. Thermogravimetric analysis of the bulk samples LP-MSN-N₃, LP-MSN-CA and LP-MSN-HRP was performed on a Netzsch STA 440 C TG/DSC with a heating rate of 10 K min⁻¹ in a stream of synthetic air of about 25 mL min⁻¹. The mass was normalized to 100% at 130 °C for all samples and the resulting data are presented in Fig. 2c. All IR measurements were performed on a Thermo Scientific Nicolet iN10 IR Microscope in reflection-absorption mode with a liquid nitrogen-cooled MCT-A detector. All spectra are background corrected. UV-vis measurements were performed on a Perkin Elmer Lambda 1050 spectrophotometer with a deuterium arc lamp (UV region) and a tungsten filament (visible region). The detector was an InGaAs integrating sphere detector. Time-based enzyme activity assays were performed in macro PMMA-cuvettes (path length 10 mm). For small sample amounts (2 µL of the sample) a NanoDrop 2000c spectrometer from Thermo Scientific Fisher was employed for UV-vis measurements. The absorbance at 280 nm (mode A280) was used to determine carbonic anhydrase concentrations.

Buffer preparation

MES buffer (0.1 M, pH 6.0). 2-(*N*-Morpholino)ethanesulfonic acid (MES, 9.76 g) was dissolved in water (500 mL). The pH was adjusted to 6.0 using sodium hydroxide (1 M).

Sodium phosphate buffer (5 mM, pH 7.4). Monosodium hydrogen phosphate (2.92 g) and disodium hydrogen phosphate (7.74 g) were dissolved in 10 L of water (5 mM). The pH was fine-adjusted to 7.4 with NaOH or HCl using a pH-meter.

Potassium phosphate buffer (0.2 M, pH 7.0). Monopotassium hydrogen phosphate (13.61 g) and dipotassium hydrogen phosphate (17.40 g) were dissolved in water (500 mL). The pH was fine-adjusted to 7.0 with NaOH or HCl using a pH-meter.

TRIS buffer (0.1 M, pH 8.0). Tris(hydroxymethyl)amino-methane (TRIS, 6.075 g) was dissolved in water (500 mL). The pH was adjusted to 8.0 using HCl (1 M).

Synthesis of alkyne-modified enzymes (sp-enzymes)

Carbonic anhydrase (sp-CA). To a freshly prepared, cooled solution (4 °C) of carbonic anhydrase (40 mg, $M_w = 29\,000\text{ g mol}^{-1}$, 1.38 µmol) in MES buffer (pH 6, 18.7 mL, 0.1 M), an aqueous solution (1 mL) of 4-pentynoic acid (0.1 M, 9.81 mg, 0.1 mmol) was added. The resulting mixture was vortexed for 2 min and then stored at 4 °C for 15 min. Subsequently, EDC (11.5 mg, 0.07 mmol) was added to the solution. The reaction was vortexed again for 2 min and then kept at 4 °C for 4 h without stirring. Afterwards, the obtained solution was dialyzed in a cold room at 4 °C against sodium phosphate buffer (5 mM, pH 7.4, 10 L) for a period of 24 h. The concentration of sp-CA (3.027 mg mL⁻¹)

was determined with Nanodrop. The alkyne-functionalized carbonic anhydrase was used for click reactions without further purification.

Horseradish peroxidase (sp-HRP). Alkyne-functionalized horseradish peroxidase was synthesized according to Gole *et al.* as described above.⁴² The concentration of sp-HRP (1.32 mg mL⁻¹) was determined with UV-vis spectroscopy (calibration curve, Fig. S2, ESI†).

Synthesis of (3-azidopropyl) triethoxysilane

(3-Azidopropyl)triethoxysilane was synthesized according to a procedure published by Nakazawa *et al.*⁴³ (3-Chloropropyl)triethoxysilane (10 g, 41.7 mmol) and sodium azide (10 g, 154 mmol) were heated in anhydrous DMF (100 mL) under inert gas conditions at 90 °C for 4 h. Low boiling materials were removed from the mixture under reduced pressure. The crude oily product was dissolved in diethyl ether, resulting in the precipitation of salts, which were removed by filtration. Et₂O was removed *in vacuo* and the residual oil was distilled (95 °C). (3-Azidopropyl)triethoxysilane was obtained as colorless liquid and used without further purification.

Synthesis of azide functionalized large pore mesoporous silica nanoparticles (LP-MSN-N₃)

Core-shell bi-functional (MSN-N_{3,in}-Ph_{out}) MSNs were synthesized through a delayed co-condensation approach based on an adapted recipe reported in the literature.¹⁸ In brief, TEA (0.047 g, 0.32 mmol), CTATos (0.263 g, 0.58 mmol) and H₂O (13.7 g, 0.77 mmol) were mixed in a 100 mL round bottom flask and stirred vigorously (1250 rpm) at 80 °C until the surfactant solution became homogeneous. TEOS (1.71 g, 8.2 mmol) and AzTES ((3-azidopropyl)triethoxysilane) (120 µL, 0.41 mmol; 5 mol%) were mixed and added to the surfactant solution and the mixture was stirred (1250 rpm) at 80 °C for 1 h. Afterwards, 201 mg of TEOS (0.96 mmol) was separated into 4 aliquots and added to the mixture every 3 minutes. The solution was further stirred for 1 h at 80 °C. A mixture of TEOS (20.1 mg, 0.096 mmol) and PhTES (phenyltriethoxysilane) (22.9 mg, 0.096 mmol, 1 mol%) was then added to the solution to generate the outer shell of the MSNs. The resulting solution was continuously stirred at 80 °C for 1 h. The as-synthesized particles were collected by centrifugation (7197g, 20 min) and were subsequently template extracted (see below).

Template removal from LP-MSN-N₃

The organic template was removed *via* extraction from LP-MSN-N₃. Thus, 1 g of the as-synthesized particles was heated in an ethanolic solution (150 mL) containing 3 g ammonium nitrate at 90 °C under reflux for 1 h, cooled and collected by centrifugation (7197g, 20 min) and extracted by a second reflux at 90 °C using a 2 M HCl/ethanolic solution (150 mL) for 1 h. Afterwards, samples were washed in the sequence EtOH, H₂O, EtOH (100 mL per wash) and were finally kept in 20 mL EtOH. Particles were collected by centrifugation (7197g, 20 min) after each template extraction and washing step.

Immobilization of alkyne-functionalized carbonic anhydrase in LP-MSN-N₃ (LP-MSN-CA)

An ethanolic suspension containing 50 mg LP-MSN-N₃ was centrifuged (10 min, 7197g), washed with 15 mL sodium phosphate buffer (0.2 M, pH 7.2) and re-dispersed in 2.5 mL sodium phosphate buffer as well as 2 mL water. The suspension was vortexed for 2 minutes and put into an ultrasonic bath for 10 minutes to agglomerates. Subsequently, the buffered solution of sp-CA (containing 9 mg, 0.3 μmol sp-CA) was added and the resulting mixture was stirred for 30 minutes at room temperature. In the meantime, sodium ascorbate (1 mg, 5.05 μmol) was added to a solution of Cu(II)SO₄ (1.25 mg, 1 mmol) dissolved in 5 mL water and stirred for 10 min at ambient temperature. 12 μL of this freshly prepared solution was added to the reaction mixture containing LP-MSN-N₃ and sp-CA to catalyze the covalent attachment of the enzyme *via* click chemistry. The resulting suspension was shaken (600 rpm) for 30 minutes at room temperature. Subsequently, the particles were collected by centrifugation (10 min, 5500g, 15 °C) and re-dispersed in 30 mL water. This washing procedure was repeated three times. LP-MSN-CA were obtained as colloidal solution in water and were stored at -20 °C until further use.

Horseradish peroxidase (LP-MSN-HRP)

Sp-Horseradish peroxidase was immobilized onto LP-MSN-N₃ *via* a click chemistry approach according to the synthesis procedure described above for sp-CA. An ethanolic suspension containing 50 mg LP-MSN-N₃ was centrifuged (10 min, 7197g), washed and re-dispersed as described above. Afterwards, the buffered solution of sp-HRP (containing 9 mg, 0.2 μmol sp-HRP) was added and the mixture was stirred for 30 minutes at room temperature before the freshly prepared catalyst solution consisting of sodium ascorbate and Cu(II)SO₄ (see above) was added. LP-MSN-HRP nanoparticles were obtained as colloidal solution in water after several washing steps.

Catalytic activity determination of LP-MSN-CA

The catalytic activity of LP-MSN-CA was determined by an adapted method published by Shank *et al.*⁴⁴ Fresh solutions of 4-nitrophenyl acetate (NPA, 10 mM, 18.1 mg, 0.1 mmol in 10 mL EtOH) and TRIS buffer (50 mM, pH 8) were prepared shortly before the experiment. 500 μL of an aqueous suspension of LP-MSN-CA (containing 5 mg particles and therefore 0.71 mg carbonic anhydrase, calculated from TGA-data) were mixed in macro PMMA-cuvettes with 400 μL TRIS buffer. Subsequently, 100 μL NPA-solution were added quickly before the time-dependent hydrolysis of the substrate was determined by measuring the absorbance of the formed 4-nitrophenol (400 nm, 120 s and intervals of 1 s). All spectra were background corrected. After a finished cycle, the assay mixture was centrifuged (10 min, 16 900g, 15 °C) and washed with 1 mL water. The washing procedure was repeated three times before the particles were re-dispersed in 500 μL water and used for the next cycle.

Catalytic activity determination of LP-MSN-HRP

To determine the catalytic activity of immobilized horseradish peroxidase (LP-MSN-HRP) a slightly modified assay following

the published protocol of Maehly and Chance was used.⁴⁵ All substrate solutions and potassium phosphate buffer (pH 7.0, 0.2 M) were freshly prepared. 5 mg LP-MSN-HRP was re-dispersed in 100 μL H₂O and 3 mL buffer as well as 50 μL guaiacol solution (0.5 mM, 2.8 μL in 50 mL water) added and mixed. Subsequently, 20 μL H₂O₂ (12.3 mM) was added, the cuvette once inverted and the time-dependent formation of the coloured product determined by UV-VIS spectroscopy (470 nm, 100 s, intervals of 1 s). All spectra were background corrected.

Results and discussion

Synthesis of large pore MSNs

For the immobilization of alkyne-functionalized enzymes by a bio-orthogonal click chemistry approach, core-shell mesoporous silica nanoparticles with large pores and azide groups on the internal and phenyl groups on the external surface (LP-MSN-N₃) were synthesized using the delayed co-condensation procedure developed in our group following a modified protocol from Zhang *et al.*^{18,46}

In brief, a delayed co-condensation approach was chosen to introduce small amounts (5 mol% of the original TEOS amount) of azide-functionality into the inside of the mesoporous framework of the LP-MSNs and to obtain a homogeneous distribution of organic moieties within the silica material to ensure immobilization of the enzymes only inside the pores of the particles. Higher degrees of organo-modification can result in a reduction of the pore diameter and would thus impede the diffusion of enzyme molecules into the mesoporous channels and increase the likelihood of pore blocking. For the introduction of azide-moieties in the core, the silica source tetraethyl orthosilicate (TEOS) was co-condensed with (3-azidopropyl)triethoxysilane (AzTES, 5 mol% of total silane content) while PhTES (1 mol% of total silane content) and TEOS were used to generate phenyl groups on the external surface. A shell of pure TEOS was condensed in-between to create an interlayer between the two different functional groups. Additionally, we found that the introduction of organo-moieties in the case of azide-silanes has no negative effect on the formation of the mesoporous structure, whereas amine-functionalities easily disrupt the large-pore nanoparticle formation. TEM and SEM micrographs (Fig. 1a-c) of the resulting core-shell particles (MSN-N_{3,in}-Ph_{out}) show a stellate morphology and a conical-like pore structure.

Transmission electron microscopy images show spherically shaped nanoparticles with a fairly homogenous particle size distribution within a size range of 60–90 nm (Fig. 1a). The large pores are present in each LP-MSN and evenly distributed over the entire nanoparticle. The particle size distribution data are in good accordance with the values obtained by dynamic light scattering, exhibiting a maximum at 150 nm (Fig. 1d). We explain the moderately increased apparent size obtained by DLS measurements compared to the TEM measurements with the larger hydrodynamic diameter of the LP-MSN-N₃ in comparison to their real size – possibly weak agglomeration is

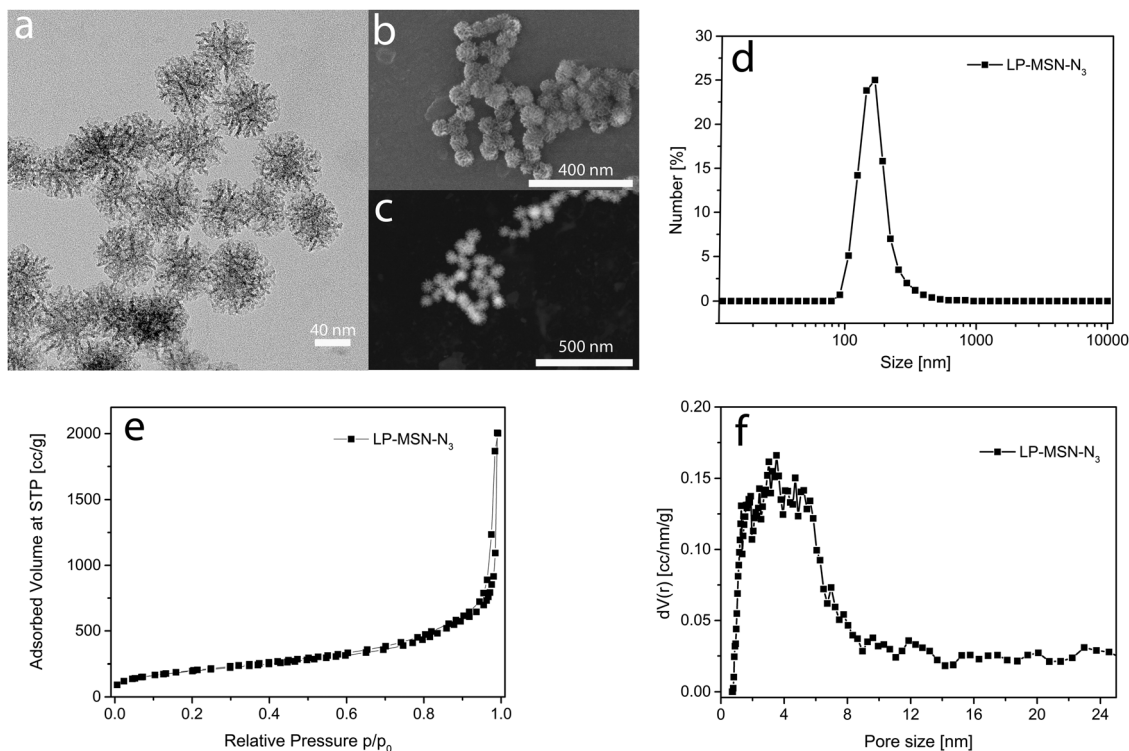


Fig. 1 Characterization of LP-MSN- N_3 . (a) Transmission electron microscopy (TEM) image, (b) scanning electron microscopy (SEM) image and (c) scanning transmission electron microscopy (STEM) image of template-extracted LP-MSN- N_3 , (d) dynamic light scattering (DLS) data showing a narrow size distribution, (e) nitrogen sorption isotherm and (f) pore size distribution obtained from nitrogen sorption measurement for LP-MSN- N_3 .

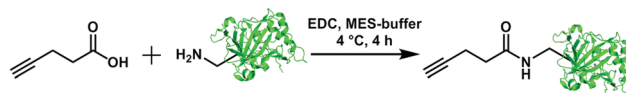
also present. The mesoporous framework is well-defined and clearly present in all particles (Fig. 1a–c). The pore sizes are in a range of about 6–10 nm (deduced from TEM measurements) and consistent with the wide pore size distribution of about 2.5–12 nm obtained from nitrogen sorption measurements (Fig. 1f). The corresponding sorption data show a hybrid isotherm of type IIb combined with a certain fraction of type IV. The narrow hysteresis can be characterized as an H3 hysteresis loop that results from aggregation and inter-granular pores and thus from a significant degree of textural porosity, indicated by the long tail in the pore size distribution (Fig. 1f). Monolayer formation of the adsorbate can be observed between $p/p_0 = 0$ and 0.2, followed by multilayer adsorption over a broad range. The apparent lack of saturation (pore filling) at high p/p_0 could be due to a broad distribution of textural porosity between the dried particles. The inter-particle voids, which are visible in the micrographs (Fig. 1a–c), are within a size-range of 10–30 nm. Summarizing, we obtained LP-MSNs exhibiting a pore size in the range of mesoporous materials (Fig. 1f, maximum around 7 nm), with a pore volume of $1.6 \text{ cm}^3 \text{ g}^{-1}$ and a BET surface area of $A_s = 670 \text{ m}^2 \text{ g}^{-1}$. In addition, infrared spectroscopy was carried out and verified the presence of azide-moieties within the pore system of LP-MSN- N_3 (Fig. S1, ESI[†]).

Immobilization of alkyne-functionalized carbonic anhydrase and horseradish peroxidase onto LP-MSN- N_3 via a click chemistry approach

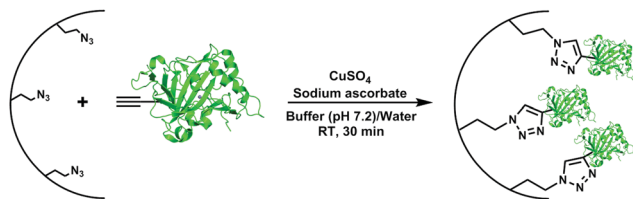
Two different enzymes, namely carbonic anhydrase (CA, 30 000 Da, $4.0 \times 4.2 \times 5.5 \text{ nm}^3$)⁴⁷ and horseradish peroxidase (HRP, 44 000 Da,

$4.0 \times 4.4 \times 6.8 \text{ nm}^3$),⁴⁸ were immobilized in the mesoporous nanoparticles. Specifically, a modified click chemistry approach was used to immobilize the enzymes within the mesoporous framework of our newly generated LP-MSNs, which required prior alkyne functionalization of the enzyme (for details see Methods section and Scheme 1).^{39,42} The latter was achieved by the EDC-activated attachment of 4-pentynoic acid to the amine moieties of CA or HRP, respectively (Scheme 1). The reaction took place in MES buffer (pH 6.0) at 4 °C.

In a second synthesis step, the LP-MSN- N_3 particles were incubated with the alkyne-functionalized enzymes for 30 minutes to ensure their diffusion into the large mesopores before the click reaction catalysts were added to the reaction mixture, in order to avoid pore blocking (for details see Methods section). Subsequently, a click reaction was performed according to a slightly modified procedure published by Himo *et al.*, employing sodium ascorbate as reducing agent for Cu(II) (CuSO_4) (Scheme 2).⁵⁰



Scheme 1 Alkyne-functionalization of enzymes. EDC activated attachment of 4-pentynoic acid to the respective enzyme (carbonic anhydrase or horseradish peroxidase; here shown with bovine carbonic anhydrase II). The reaction was carried out in MES buffer (pH 6.0) at 4 °C. The accession number from the protein data bank (PDB) for the X-ray structure of BCII is 1V9E.⁴⁹



Scheme 2 Covalent attachment of sp-enzymes into LP-MSN- N_3 . Scheme for protein immobilization in LP-MSNs using click chemistry. Cu(II) was reduced with sodium ascorbate resulting in Cu(I), the actual catalyst.

The nanoparticles were washed several times with water in order to remove excess and unbound enzyme molecules.

All obtained nitrogen sorption data show isotherms that appear as hybrids between type II and type IV isotherms, with a narrow H3 hysteresis loop. After the attachment of sp-enzymes the calculated BET-surface decreased significantly (Fig. 2a and Table 1 respectively). This can be attributed to the uptake and covalent immobilization of the enzyme molecules within the large mesopores of the nanoparticles and the resulting partial pore filling. Accordingly, the pore volume decreased likewise (Fig. 2b). A strong reduction of the very small pore sizes can be observed. We attribute this to the conical-like shape of the pores: enzymes that diffuse entirely into the pore, block the small end of it and thereby the parts of the pores representing small pore sizes. Carbonic anhydrase shows a stronger reduction of the smaller pore sizes than horseradish peroxidase, possibly due to their different shape: the shape of CA is close to a square and thus, when it gets stuck in a pore due to size limitations, it may block the entire pore uniformly in all directions. HRP is rod-shaped, if it blocks a pore there is space on its sides that allows for BET measurements to still access and

probe the pore. We assume that the decrease in pore volume in case of the sample LP-MSN-CA is stronger than in LP-MSN-HRP because a larger amount of sp-CA could be incorporated into the mesoporous framework of our nanoparticles. These results are in good accordance with the thermogravimetric analysis (TGA) data (Fig. 1c and Table 1 for relative mass loss), showing that more carbonic anhydrase than horseradish peroxidase was immobilized in the LP-MSNs. The higher degree of immobilization of CA as compared to HRP is attributed to its smaller dimension; the enzyme can diffuse more easily into the mesopores without having as much contact with the pore walls and the attached organic moieties, while HRP is bigger and thus has a higher likelihood to touch the pore walls, bind to them and block access to the pore for additional molecules.

From the additional mass loss of 11.5% for the sample LP-MSN-CA compared to LP-MSN- N_3 , the amount of attached enzyme can be estimated to be 4.7 μmol per g silica (for calculation see Calculation A1 in the ESI[†]), which corresponds to 141 mg carbonic anhydrase per g silica support. The amount was additionally determined *via* Bradford assay, resulting in 99 mg CA per g silica (see ESI[†], Fig. S10). This deviation of almost 28% is attributed to additional components in the channels of the mesoporous silica that contribute to weight changes during TGA measurements. The determined amount indicates that 0.5% of all azide-moieties have reacted with sp-CA, as the amount of azide-moieties was estimated to 1.02 mmol per g silica. From the additional mass loss of 9.4% for the sample LP-MSN-HRP compared to the azide-functionalized LP-MSNs, the amount of immobilized horseradish peroxidase can be estimated to 2.6 μmol per g silica (see ESI[†], Calculation A1), or to 114 mg HRP per g silica support. The amount determined with the additionally performed Bradford assay (see ESI[†], Fig. S11)

Table 1 Nitrogen physisorption and thermogravimetric analysis data of LP-MSN- N_3 and LP-MSN-enzyme

Sample	BET surface area [$\text{m}^2 \text{g}^{-1}$]	Pore size range ^a [nm]	Pore volume [$\text{cm}^3 \text{g}^{-1}$]	Relative mass loss ^b [%]
LP-MSN- N_3	670	2.5–12	1.6	9.2 (7.7% for N_3 -moieties)
LP-MSN-CA	389	5.5–12	1.2	20.7
LP-MSN-HRP	423	5.3–12	1.4	18.6

^a DFT pore size range refers to the main range of the pore size distribution. ^b Relative mass loss obtained by TGA; all curves are normalized to 130 °C.

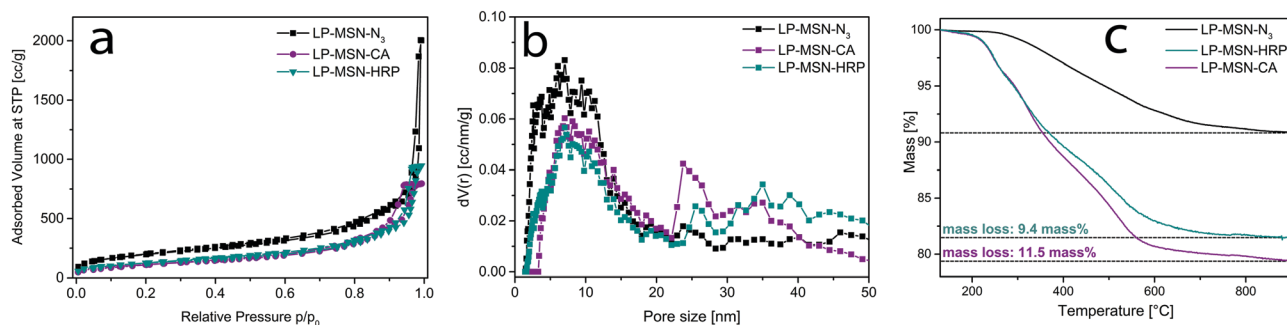


Fig. 2 Nitrogen sorption data of LP-MSN- N_3 with immobilized enzymes. (a) Isotherm of LP-MSN- N_3 (black), LP-MSN-CA (purple) and LP-MSN-HRP (cyan). (b) Pore size distribution for LP-MSN- N_3 (black), LP-MSN-CA (purple) and LP-MSN-HRP (cyan). (c) Thermogravimetric analysis data of LP-MSN- N_3 (black), LP-MSN-HRP (cyan) and LP-MSN-CA (purple). All TGA curves are normalized to 100% at 130 °C.

differs very little from the above TGA results and corresponds to 103 mg HRP per g silica. This indicates that a smaller amount of sp-Horseradish peroxidase molecules was able to diffuse into the large mesopores and reacted with 0.25% of all azide-moieties of LP-MSN-N₃. A probable reason for this is the even larger molecular dimension of horseradish peroxidase ($4.0 \times 4.4 \times 6.8 \text{ nm}^3$),⁴⁸ resulting in partial blocking of the pores by immobilized horseradish peroxidase. All nitrogen sorption data are supported by the corresponding thermogravimetric analysis and the calculated relative mass losses that are summarized in Table 1. As further proof for the successful attachment of sp-enzymes *via* click chemistry, vibrational spectroscopy was performed with the respective LP-MSN-enzyme samples (see Fig. S3 for CA and S4 for HRP, ESI†). The symmetric and asymmetric CH₂ stretching vibrations of the enzyme appear in the range of 2960–2871 cm⁻¹ in the spectrum of LP-MSN-CA and sp-CA and of LP-MSN-HRP and sp-HRP, respectively. The peak at 2105 cm⁻¹ can be attributed to the asymmetric N₃ stretching vibration of LP-MSN-N₃ and can still be observed in LP-MSN-enzyme due to the small fraction of reacted (clicked) azide-moieties. At 1658 cm⁻¹ (dashed line) the C=O stretching vibration appears in the spectrum of LP-MSN-CA/HRP, which is attributed to the amide bonds of the attached enzymes. The vibration at 1530 cm⁻¹ (second dashed line) is only visible in the spectra of sp-enzyme and LP-MSN-enzyme and represents the N-H bending vibration of the peptide bonds of the enzyme. The peak at 1627 cm⁻¹ in the spectrum of LP-MSN-N₃ indicates the presence of traces of water within the sample. Below 1300 cm⁻¹, vibrations of the silica framework appear with strong intensity. Summarizing, the results obtained by nitrogen sorption, thermogravimetric analysis and vibrational spectroscopy all support the successful immobilization of carbonic anhydrase and horseradish peroxidase within the porous network of LP-MSN-N₃. In the following we address the catalytic properties of the immobilized enzymes.

Catalytic activity determination of immobilized carbonic anhydrase

To characterize the properties of immobilized CA, the catalytic activity of the hydrolysis of 4-nitrophenylacetate (NPA) was studied colorimetrically by measuring the absorbance of the newly formed yellow nitrophenol at 400 nm (Fig. 3a and Fig. S5, ESI†). To ascertain the robust attachment and stability of the enzyme inside the pores, multiple cycles were performed. After cycle 1, the reaction mixture was transferred to small Eppendorf tubes and centrifuged for 5 min (15 °C, 16 900g). The pellet was redispersed in water and centrifuged again. This washing step was conducted two times to remove (un)reacted substrate. Afterwards, the washed particles were redispersed in water and fresh substrate was added for the next cycle. In total eight such cycles with intermediate washing steps were performed (Fig. 3a). The time-based measurements show a successful conversion of 4-NPA to nitrophenol in all cycles, proving the continuous activity and stability of the immobilized carbonic anhydrase. Due to the washing steps in between the cycles, a certain loss of particles and therefore also enzyme can be seen by a decrease in

pellet size and accordingly a decrease in absorbance and slope (Fig. 3a). The self-hydrolysis of 4-NPA was measured separately (data shown in Fig. S6, ESI†). The self-hydrolysis reaction data were subtracted from the raw data of the enzyme-catalyzed hydrolysis. In Fig. 3a and Fig. S7 (ESI†) the CA activity corrected for self-hydrolysis is shown. For quantitative determination of the reaction rate, the slope of one cycle at a reduced substrate concentration (1 mM NPA) was converted into concentration *vs.* time (Fig. S7, ESI†) by using Lambert-Beer's law ($\epsilon = 16300 \text{ M}^{-1} \text{ cm}^{-1}$).⁵¹ According to Michaelis-Menten kinetics in the limit of low substrate concentrations, the kinetic constant k_{cat}/K_m was determined to be $74 \text{ M}^{-1} \text{ s}^{-1}$. There are large differences in the kinetic constants for different CAs reported in the literature.⁵² Therefore, it is difficult to compare our result for immobilized bovine carbonic anhydrase to literature values.

The resulting activity of immobilized carbonic anhydrase was also determined in international units IU, which is described in the ESI.† The expressed activity of the biocatalyst LP-MSN-CA results in 8.4 units (per 5 mg MSNs) *i.e.* 1680 units per g support. The corresponding amount of free enzyme shows an activity of 85.6 units and therefore performs one order of magnitude faster than the immobilized enzyme, which might be attributed to partial blocking of the enzyme due to the statistical attachment of the enzyme molecules inside the pores. All in all, it could be shown that carbonic anhydrase was successfully immobilized inside the large pores of our MSNs and remained there stable and active.

Horseradish peroxidase activity determination

In order to determine the catalytic activity of the MSN-bound HRP molecules, an assay involving the oxidation of guaiacol was performed.⁴⁵ Thereby, the catalyzed oxidation of guaiacol was measured by recording the absorption of the produced tetraguaiacol at 470 nm with UV-vis spectroscopy (Fig. 3b, for experimental details see Methods section and Fig. S8, ESI†). The remaining stability and activity of the immobilized enzyme could be shown over several cycles just as well as in the case of carbonic anhydrase. To determine the reaction rate, the slope in the linear region (0 s–15 s) of the first cycle's graph (gray graph) was used and converted into concentration *vs.* time (Fig. S9, ESI†) using Lambert-Beer's law (with $\epsilon = 26.6 \text{ mM}^{-1} \text{ cm}^{-1}$ from Maehly and Chance⁴⁵ and $d = 1 \text{ cm}$). The rate was calculated to be $2.5 \times 10^4 \text{ M}^{-1} \text{ cm}^{-1}$ according to Maehly and Chance.⁴⁵ In comparison to the literature value⁴⁵ of $3 \times 10^5 \text{ M}^{-1} \text{ cm}^{-1}$, our immobilized enzyme performs slower by about one order of magnitude than the free corresponding sp-enzyme. The resulting activity of immobilized horseradish peroxidase (definitions of IU at the end of the ESI†) is 0.86 units (per 0.16 mg MSN) *i.e.* 5343 units per g support. The corresponding amount of free enzyme shows an activity of 3.7 units, resulting in an only fourfold better performance than our immobilized HRP.

Note that the enzyme concentration used in the calculations is the upper limit. Due to a necessary centrifugation step before the activity assay a small loss of particles and therefore enzyme is inevitable, thus reducing the enzyme concentration. Since the enzyme concentration is inversely proportional to the

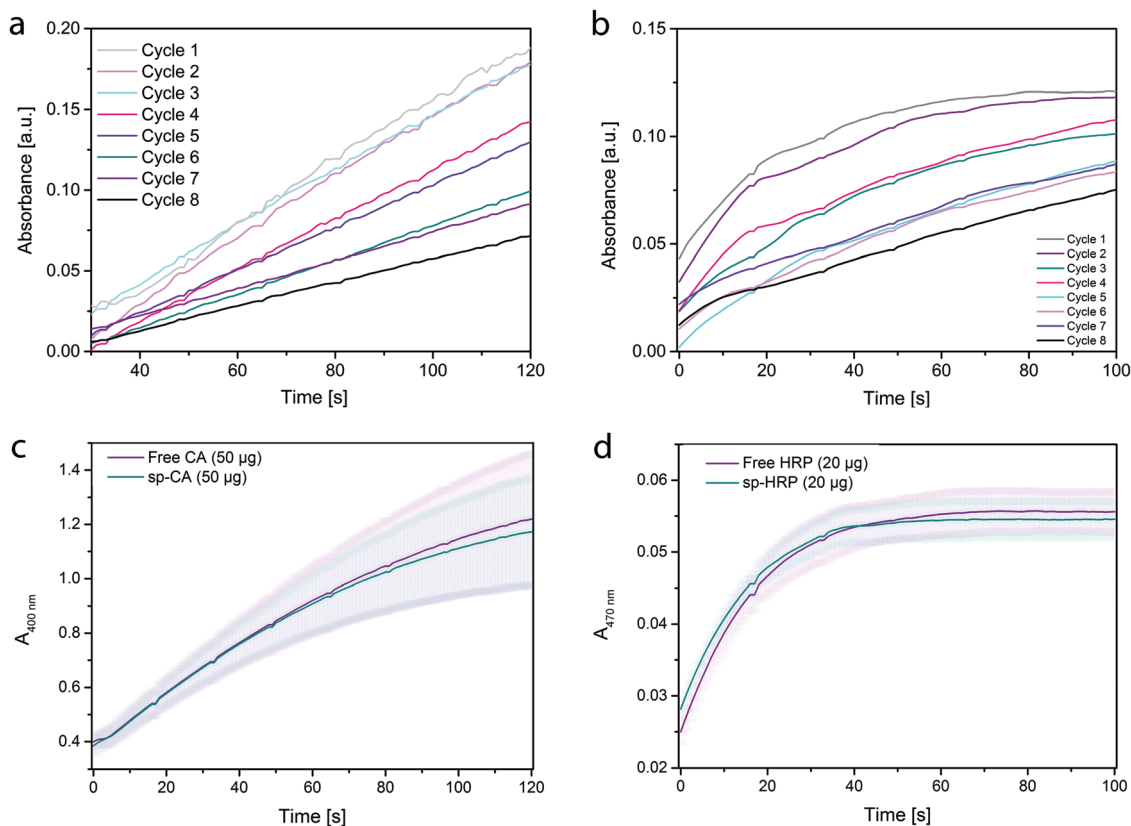


Fig. 3 Activity determination for LP-MSN-CA and LP-MSN-HRP as well as for free versus alkyne-functionalized enzymes. (a) UV-vis absorption measurement of catalyzed hydrolysis of the substrate 4-nitrophenol acetate (NPA) by LP-MSN-CA within a period of 120 s (interval 1 s) at 400 nm with 10 mM NPA in TRIS buffer (pH 8, 50 mM) over eight cycles. (b) Activity determination of LP-MSN-HRP by measuring the absorbance at 470 nm of emerging oxidized guaiacol (2-methoxyphenol) in potassium phosphate buffer (pH 7, 0.2 M) for 100 s (interval 1 s) over eight catalytic cycles. The enzyme's reaction rate was determined from the slope of the first cycle's linear region (gray curve, from 0 s–15 s). (c) Catalytic activity of native versus functionalized carbonic anhydrase (assay described in (a)). Comparison of catalytic activity of native (free) CA (purple line \pm SD light purple area) versus functionalized CA (sp-CA) (cyan line \pm SD light cyan area). (d) Activity comparison of native versus functionalized horseradish peroxidase (assay described in (b)). Activity determination of native (free) HRP (purple line \pm SD light purple area) versus sp-HRP (cyan line \pm SD light cyan area) by measuring the absorbance of oxidized guaiacol at 470 nm for 100 s.

calculated reaction rate, our value of the calculated reaction rate represents a lower limit. Additionally, some horseradish peroxidase molecules could be partially hindered or blocked due to the random attachment of the large enzymes into the rather tightly matching pores; the active center might not always be perfectly accessible for the substrates. This may explain the lower reaction rate in comparison to unbound HRP.

To prove that alkyne-functionalisation of the enzymes does not impair their catalytic activity, the activity assays were performed with the native versus alkyne-functionalized enzymes. In both cases (Fig. 3c and d) it can be shown that the catalytic performance is maintained after enzyme-functionalization.

Conclusion

We report a facile delayed co-condensation strategy for the synthesis of spatially segregated core-shell bi-functional large-pore MSNs. This direct approach towards introducing organo-moieties into the mesopores is highly beneficial since different

functionalities can be efficiently introduced at controlled concentrations. This method further avoids additional grafting steps that may be difficult with colloidal systems. Our synthesis yields mesoporous silica nanoparticles within a size range of about 100 nm exhibiting large pore sizes of up to 12 nm and carrying azide-functionalities inside the pore system. This organo-functionalization makes the LP-MSNs suitable for a biocompatible modification *via* click chemistry. We covalently immobilized the two enzymes carbonic anhydrase and horseradish peroxidase in the interior of the LP-MSN- N_3 host.

The lyase carbonic anhydrase (CA) ($4.0 \times 4.2 \times 5.5 \text{ nm}^3$)⁴⁷ and the peroxidase horseradish peroxidase (HRP) ($4.0 \times 4.4 \times 6.8 \text{ nm}^3$)⁴⁸ were successfully modified with alkyne-linkers to enable grafting through a Cu-catalyzed click reaction. The enzymes were allowed to diffuse into the mesopores before the catalysts for the click reaction were added to the reaction mixture, thus avoiding unfavorable pore blocking and low catalytic activity. We could demonstrate in this study that both enzymes are still highly active in their immobilized state, and that they maintain high activity during activity assays over several cycles.

Overall, we present a spatially structured colloidal MSN-based system with large pores for the immobilization of active biomolecules that holds promise as a versatile platform for numerous applications.

Conflicts of interest

The authors declare no competing financial interest.

Acknowledgements

Financial support from the German Science Foundation (DFG) (Cluster Nanosystems Initiative Munich (NIM) and SFB 1032, project B05) and the Center for NanoScience Munich (CeNS) is gratefully acknowledged. We thank Dr Steffen Schmidt for electron microscopy.

References

- 1 Y. Lu, H. Fan, A. Stump, T. L. Ward, T. Rieker and C. J. Brinker, Aerosol-Assisted Self-Assembly of Mesoporous Spherical Nanoparticles, *Nature*, 1999, **398**, 223–226.
- 2 M. Hartmann, Ordered Mesoporous Materials for Bioadsorption and Biocatalysis, *Chem. Mater.*, 2005, **17**, 4577–4593.
- 3 V. Cauda, A. Schlossbauer, J. Kecht, A. Zürner and T. Bein, Multiple Core-Shell Functionalized Colloidal Mesoporous Silica Nanoparticles, *J. Am. Chem. Soc.*, 2009, **131**, 11361–11370.
- 4 F. Gao, P. Botella, A. Corma, J. Blesa and L. Dong, Monodispersed Mesoporous Silica Nanoparticles with Very Large Pores for Enhanced Adsorption and Release of DNA, *J. Phys. Chem. B*, 2009, **113**, 1796–1804.
- 5 D. Zhao, J. Feng, Q. Huo, N. Melosh, G. H. Fredrickson, B. F. Chmelka and G. D. Stucky, Triblock copolymer syntheses of mesoporous silica with periodic 50 to 300 angstrom pores, *Science*, 1998, **279**, 548–552.
- 6 D. Zhao, Q. Huo, J. Feng, B. F. Chmelka and G. D. Stucky, Nonionic Triblock and Star Diblock Copolymer and Oligomeric Surfactant Syntheses of Highly Ordered, Hydrothermally Stable, Mesoporous Silica Structures, *J. Am. Chem. Soc.*, 1998, **120**, 6024–6036.
- 7 J. M. Rosenholm, A. Meinander, E. Peuhu, R. Niemi, J. E. Eriksson, C. Sahlgren and M. Linden, Targeting of Porous Hybrid Silica Nanoparticles to Cancer Cells, *ACS Nano*, 2009, **3**, 197–206.
- 8 Z. Zhou, R. N. K. Taylor, S. Kullmann, H. Bao and M. Hartmann, Mesoporous Organosilicas with Large Cage-Like Pores for High Efficiency Immobilization of Enzymes, *Adv. Mater.*, 2011, **23**, 2627–2632.
- 9 M. Mureseanu, A. Galarneau, G. Renard and F. Fajula, A New Mesoporous Micelle-Templated Silica Route for Enzyme Encapsulation, *Langmuir*, 2005, **21**, 4648–4655.
- 10 Y. S. Lin, N. Abadeer, K. R. Hurley and C. L. Haynes, Ultrastable, redispersible, small, and highly organomodified mesoporous silica nanotherapeutics, *J. Am. Chem. Soc.*, 2011, **133**, 20444–20457.
- 11 H. Jin, H. Qiu, Y. Sakamoto, P. Shu, O. Terasaki and S. Che, Mesoporous Silicas by Self-Assembly of Lipid Molecules: Ribbon, Hollow Sphere, and Chiral Materials, *Chem. – Eur. J.*, 2008, **14**, 6413–6420.
- 12 Y. S. Lin and C. L. Haynes, Impacts of Mesoporous Silica Nanoparticle Size, Pore Ordering, and Pore Integrity on Hemolytic Activity, *J. Am. Chem. Soc.*, 2010, **132**, 4834–4842.
- 13 S. H. Wu, C. Y. Mou and H. P. Lin, Synthesis of Mesoporous Silica Nanoparticles, *Chem. Soc. Rev.*, 2013, **42**, 3862–3875.
- 14 Y. Han and J. Y. Ying, Generalized Fluorocarbon-Surfactant-Mediated Synthesis of Nanoparticles with Various Mesoporous Structures, *Angew. Chem., Int. Ed.*, 2005, **44**, 288–292.
- 15 K. Möller, K. Müller, H. Engelke, C. Bräuchle, E. Wagner and T. Bein, Highly efficient siRNA delivery from core-shell mesoporous silica nanoparticles with multifunctional polymer caps, *Nanoscale*, 2016, **8**, 4007–4019.
- 16 S. B. Hartono, W. Gu, F. Kleitz, J. Liu, L. He, A. P. J. Middelberg, C. Yu, G. Q. Lu and S. Z. Qiao, Poly-L-lysine Functionalized Large Pore Cubic Mesoporous Silica Nanoparticles as Biocompatible Carriers for Gene Delivery, *ACS Nano*, 2012, **6**, 2104–2117.
- 17 H.-K. Na, M.-H. Kim, K. Park, S.-R. Ryoo, K. E. Lee, H. Jeon, R. Ryoo, C. Hyeon and D.-H. Min, Efficient Functional Delivery of siRNA using Mesoporous Silica Nanoparticles with Ultralarge Pores, *Small*, 2012, **8**, 1752–1761.
- 18 K. Zhang, L. L. Xu, J. G. Jiang, N. Calin, K. F. Lam, S. J. Zhang, H. H. Wu, G. D. Wu, B. Albela, L. Bonneviot and P. Wu, Facile large-scale synthesis of monodisperse mesoporous silica nanospheres with tunable pore structure, *J. Am. Chem. Soc.*, 2013, **135**, 2427–2430.
- 19 H. Y. Chiu, W. Deng, H. Engelke, J. Helma, H. Leonhardt and T. Bein, Intracellular chromobody delivery by mesoporous silica nanoparticles for antigen targeting and visualization in real time, *Sci. Rep.*, 2016, **6**, 25019.
- 20 J. Kim, J. W. Grate and P. Wang, Nanostructures for Enzyme Stabilization, *Chem. Eng. Sci.*, 2006, **61**, 1017–1026.
- 21 X. S. Zhao, X. Y. Bao, W. Guo and F. Y. Lee, Immobilizing Catalysts on Porous Materials, *Mater. Today*, 2006, **9**, 32–39.
- 22 L. T. Phuoc, P. Laveille, F. Chamouveau, G. Renard, J. Drone, B. Coq, F. Fajula and A. Galarneau, Phospholipid-templated silica nanocapsules as efficient polyenzymatic biocatalysts, *Dalton Trans.*, 2010, **39**, 8511–8520.
- 23 C. Ispas, I. Sokolov and S. Andreescu, Enzyme-functionalized Mesoporous Silica for Bioanalytical Applications, *Anal. Bioanal. Chem.*, 2009, **393**, 543–554.
- 24 Z. Li, J. C. Barnes, A. Bosoy, J. F. Stoddart and J. I. Zink, Mesoporous Silica Nanoparticles in Biomedical Applications, *Chem. Soc. Rev.*, 2012, **41**, 2590–2605.
- 25 Z. Zhou and M. Hartmann, Progress in Enzyme Immobilization in Ordered Mesoporous Materials and Related Applications, *Chem. Soc. Rev.*, 2013, **42**, 3894–3912.
- 26 H. H. P. Yiu and P. A. Wright, Enzymes Supported on Ordered Mesoporous Solids: A Special Case of an Inorganic-Organic Hybrid, *J. Mater. Chem.*, 2005, **15**, 3690–3700.
- 27 X. Y. Yang, Z. Q. Li, B. Liu, A. Klein-Hofmann, G. Tian, Y. F. Feng, Y. Ding, D. S. Su and F. S. Xiao, “Fish-in-Net”

- Encapsulation of Enzymes in Macroporous Cages for Stable, Reusable, and Active Heterogeneous Biocatalysts, *Adv. Mater.*, 2006, **18**, 410–414.
- 28 M. C. Rosales-Hernández, J. E. Mendieta-Wejebe, J. Correa-Basurto, J. I. Vázquez-Alcántara, E. Terres-Rojas and J. Trujillo-Ferrara, Catalytic Activity of Acetylcholinesterase Immobilized on Mesoporous Molecular Sieves, *Int. J. Biol. Macromol.*, 2007, **40**, 444–448.
- 29 S. Hudson, J. Cooney, B. K. Hodnett and E. Magner, Chloroperoxidase on Periodic Mesoporous Organosilanes: Immobilization and Reuse, *Chem. Mater.*, 2007, **19**, 2049–2055.
- 30 C. Lei, Y. Shin, J. Liu and E. J. Ackerman, Entrapping Enzyme in a Functionalized Nanoporous Support, *J. Am. Chem. Soc.*, 2002, **124**, 11242–11243.
- 31 F. Hoffmann, M. Cornelius, J. Morell and M. Fröba, Silica-Based Mesoporous Organic–Inorganic Hybrid Materials, *Angew. Chem., Int. Ed.*, 2006, **45**, 3216–3251.
- 32 Z. Zhou, A. Inayat, W. Schwieger and M. Hartmann, Improved activity and stability of lipase immobilized in cage-like large pore mesoporous organosilicas, *Microporous Mesoporous Mater.*, 2012, **154**, 133–141.
- 33 D. I. Fried, F. J. Brieler and M. Fröba, Designing Inorganic Porous Materials for Enzyme Adsorption and Applications in Biocatalysis, *ChemCatChem*, 2013, **5**, 862–884.
- 34 C.-H. Lee, T.-S. Lin and C.-Y. Mou, Mesoporous Materials for Encapsulating Enzymes, *Nano Today*, 2009, **4**, 165–179.
- 35 M. N. El-Nahass, M. M. El-Keiy and E. M. M. Ali, Immobilization of horseradish peroxidase into cubic mesoporous silicate, SBA-16 with high activity and enhanced stability, *Int. J. Biol. Macromol.*, 2018, **116**, 1304–1309.
- 36 F. Pitzalis, M. Monduzzi and A. Salis, A bienzymatic biocatalyst constituted by glucose oxidase and Horseradish peroxidase immobilized on ordered mesoporous silica, *Microporous Mesoporous Mater.*, 2017, **241**, 145–154.
- 37 Q. Chang and H. Tang, Immobilization of horseradish peroxidase on NH₂-modified magnetic Fe₃O₄/SiO₂ particles and its application in removal of 2,4-dichlorophenol, *Molecules*, 2014, **19**, 15768–15782.
- 38 T. Takigawa and Y. Endo, Effects of Glutaraldehyde Exposure on Human Health, *J. Occup. Health*, 2006, **48**, 75–87.
- 39 A. Schlossbauer, D. Schaffert, J. Kecht, E. Wagner and T. Bein, Click Chemistry for High-Density Biofunctionalization of Mesoporous Silica, *J. Am. Chem. Soc.*, 2008, **130**, 12558–12559.
- 40 D. I. Fried, A. Schlossbauer and T. Bein, Immobilizing Glycopyranose on Mesoporous Silica via “Click-Chemistry” for Borate Adsorption, *Microporous Mesoporous Mater.*, 2011, **147**, 5–9.
- 41 M. Yoshimoto and P. Walde, Immobilized carbonic anhydrase: preparation, characteristics and biotechnological applications, *World J. Microbiol. Biotechnol.*, 2018, **34**, 151.
- 42 A. Gole and C. J. Murphy, Azide-Derivatized Gold Nanorods: Functional Materials for “Click” Chemistry, *Langmuir*, 2007, **24**, 266–272.
- 43 J. Nakazawa and T. D. Stack, Controlled Loadings in a Mesoporous Material: Click-on Silica, *J. Am. Chem. Soc.*, 2008, **130**, 14360–14361.
- 44 R. P. Shank, D. F. McComsey, V. L. Smith-Swintosky and B. E. Maryanoff, Examination of Two Independent Kinetic Assays for Determining the Inhibition of Carbonic Anhydrases I and II: Structure–Activity Comparison of Sulfamates and Sulfamides, *Chem. Biol. Drug Des.*, 2006, 113–119.
- 45 A. C. Maehly and B. Chance, The assay of catalases and peroxidases, *Methods Biochem. Anal.*, 1954, **1**, 357–424.
- 46 H.-Y. Chiu, D. Gößl, L. Haddick, H. Engelke and T. Bein, Clickable Multifunctional Large-Pore Mesoporous Silica Nanoparticles as Nanocarriers, *Chem. Mater.*, 2018, **30**, 644–654.
- 47 V. M. Krishnamurthy, G. K. Kaufman, A. R. Urbach, I. Gitlin, K. L. Gudiksen, D. B. Weibel and G. M. Whitesides, Carbonic Anhydrase as a Model for Biophysical and Physical–Organic Studies of Proteins and Protein–Ligand Binding, *Chem. Rev.*, 2008, **108**, 946–1051.
- 48 S. Hudson, J. Cooney and E. Magner, Proteins in mesoporous silicates, *Angew. Chem., Int. Ed. Engl.*, 2008, **47**, 8582–8594.
- 49 R. Saito, T. Sato, A. Ikai and N. Tanaka, Structure of bovine carbonic anhydrase II at 1.95 Å resolution, *Acta Crystallogr., Sect. D: Biol. Crystallogr.*, 2004, **60**, 792–795.
- 50 F. Himo, T. Lovell, R. Hilgraf, V. V. Rostovtsev, L. Noodleman, K. B. Sharpless and V. V. Fokin, Copper(I)-catalyzed synthesis of azoles. DFT study predicts unprecedented reactivity and intermediates, *J. Am. Chem. Soc.*, 2005, **127**, 210–216.
- 51 J. A. Verpoorte, S. Mehta and J. T. Edsall, Esterase Activities of Human Carbonic Anhydrases B and C, *J. Biol. Chem.*, 1967, **242**, 4221–4229.
- 52 E. Ozdemir, Biomimetic CO₂ Sequestration: 1. Immobilization of Carbonic Anhydrase within Polyurethane Foam, *Energy Fuels*, 2009, **23**, 5725–5730.